HAL

archives-ouvertes.fr

Stable isotope characterization of pedogenic and lacustrine carbonates from the Chinese Tian Shan: constraints on the Mesozoic - Lower Cenozoic palaeo-environmental evolution

Gloria Heilbronn, Philippe Boulvais, E Marchand, Cécile Robin, Sylvie Bourquin, Laurie Barrier, Y Jia, B. Fu, Marc Jolivet

▶ To cite this version:

HAL Id: insu-01116934

https://hal-insu.archives-ouvertes.fr/insu-01116934

Submitted on 22 Jun 2015

1   Stable isotope characterization of pedogenic and lacustrine carbonates from the Chinese Tian Shan:

2   constraints on the Mesozoic – Lower Cenozoic palaeo-environmental evolution

3

4   Heilbronn G. [(1)], Boulvais P. [(1)], Marchand E. [(1)], Robin C. [(1)], Bourquin S. [(1)], Barrier L. [(2)], Jia Y. [(3)], Fu B.

5   [(3)], Jolivet M [(1)].

6

7   (1) Géosciences Rennes, Observatoire des Sciences de l'Univers de Rennes, UMR 6118 CNRS –

8   Univ. Rennes 1, Rennes, France.

9   (2) Institut de Physique du Globe de Paris, Sorbonne Paris Cité, Université Paris Diderot, UMR

10   CNRS 7154, 1 rue Jussieu, F-75005 Paris, France.

11   (3) Center for Earth Observation and Digital Earth, Chinese Academy of Sciences, Beijing, China.

12

13

15

16   Abstract

17   In the Mesozoic-Cenozoic continental deposits of the Tian Shan area, two main levels containing

18   pedogenic carbonates have been identified on both the southern and northern foothills of the range:

19   one in the Upper Jurassic series and one in the Upper Cretaceous - Lower Palaeocene series. In order

20   to reconstruct the palaeo-environmental and palaeo-topographic characteristics of the Tian Shan

21   area during these two periods, we measured the oxygen and carbon isotope composition of these

22   pedogenic carbonates (calcrete and nodules). The stable isotope compositions are homogeneous:

23   most $\delta^{18}O$ values are between 21 and 25‰ and most $\delta^{13}C$ values are between -4 and -6‰. No

24   distinction can be made between the calcrete and nodule isotopic compositions. The constancy of

25   isotopic values across the Tian Shan is evidence of a development of these calcification features in

26   similar palaeo-environmental conditions. The main inference is that no significant relief existed in

27   that area at the Cretaceous - Palaeogene boundary, implying that most of the present relief

28   developed later, during the Cenozoic. In addition to the pedogenic carbonates, few beds of

29   limestones interstratified in the Jurassic series of the southern foothills display oxygen and carbon

30 isotope compositions typical of lacustrine carbonates, ruling out brackish water incursion at that
31 period in the region.

32

34

1. Introduction

36 Calcification is a ubiquitous phenomenon that occurs in a large variety of geological settings
37 including limestone diagenesis and continental weathering. In continental environments, under semi-
38 arid conditions, the interaction between meteoric waters or groundwaters and sedimentary rocks
39 commonly leads to pedogenic calcification (e.g. Wright and Tucker, 1991; Alonso-Zarza, 2003;
40 Hasiotis et al., 2007). The resulting calcareous features correspond to the so-called calcretes and
41 occur as isolated nodules or rather continuous levels of carbonates (Retallack, 1997; Wright, 2008).
42 The oxygen and carbon isotope composition of such neo-formed carbonates provides information on
43 the palaeo-environments within which they precipitated (e.g. Alonso-Zarza, 2003). Indeed, while the
44 oxygen isotope composition of these carbonates depends upon processes taking place in the soil –
45 ground water system, such as evaporation, it is also function of the composition of the meteoric
46 water. The later depends on the palaeo-latitude and the palaeo-altitude of the area, as well as on the
47 distance to the ocean from which the atmospheric masses are derived. In a specific region, any
48 variation in the δ^{18}O value of the carbonates through time may thus be, for example, a consequence
49 of the climatic evolution. At a specific stratigraphic level, geographic variations of δ^{18}O may relate to
50 the existence of a significant palaeo-topography (e.g. Garzione et al., 2000). In a similar way, the
51 carbon isotope composition of continental neo-formed carbonates depends on the source of the
52 carbon in the region, which relates to the relative abundance of carbon-bearing rocks (e.g. marine
53 carbonates) over available organic carbon. The former have δ^{13}C values close to 0‰, whereas the
54 second source has very negative values, close to -25‰ for carbon derived from C3-type plants and -
55 15‰ from C4-type ones. The δ^{13}C signal can thus potentially be related to the geology of the area,
56 the palaeo-flora itself partially controlled by the palaeo-climate (e.g. Pustovoytov, 2002).

57 In North-West China, the intracontinental, east-west oriented Tian Shan Range (Fig. 1) provides
58 spectacular outcrops of Mesozoic-Cenozoic clastic sediment series. During fieldwork, we recognized
59 several occurrences of calcretes and nodules throughout these series, especially in the Upper
60 Mesozoic and Lower Cenozoic deposits. A strong aridification occurred during Late Jurassic, following

61　the progressive appearance of dry seasons since the late Early Jurassic (e.g. Allen et al., 1991;

62　Hendrix et al., 1992; Eberth et al., 2001; Li et al., 2004; Ashraf et al., 2010; Pan et al., 2012). Since this

63　period, arid to semi-arid climate has been predominant in the Tian Shan area (e.g. Allen et al., 1991;

64　Hendrix et al., 1992; Li et al., 2004; Sun and Wang, 2005; Jiang et al., 2008).

65　Since the late 1970s, the Cenozoic tectonic development of the range and its foreland basins has

66　been widely studied (e.g. Tapponnier and Molnar, 1979; Windley et al., 1990; Allen et al., 1991;

67　Hendrix et al., 1994; Charreau et al., 2005, 2009, 2012; Jolivet et al., 2014). In contrast, the Mesozoic

68　evolution of the Tian Shan area is still largely debated (Jolivet et al., 2013), despite some efforts to

69　reconstruct the sedimentary depositional environments (e.g. Hendrix et al., 1992; Li et al., 2004;

70　Eberth et al., 2001; Vincent and Allen, 2001; Sha et al., 2011), the palaeo-topographic evolution

71　(Dumitru et al., 2001; Jolivet et al., 2010; Yang et al., 2013; D. Liu et al., 2013; Yang et al., n.d. in

72　press) and the palaeo-climate (e.g. Hendrix et al., 1992, 1994; Hendrix, 2000; Eberth et al., 2001; Li et

73　al., 2004; Ashraf et al., 2010; Bian et al., 2010). In this paper, we provide new isotopic data on

74　pedogenic carbonates (calcrete and nodules) and limestone beds in order to improve our

75　understanding of the general evolution of the area from Late Jurassic to Early Palaeogene.

76

2. Geological setting

78　　　The Tian Shan is a large mountain belt extending in Central Asia through Kyrgyzstan,

79　Kazakhstan and North-West China (Fig. 1a). This range is surrounded by several basins among which

80　the Junggar Basin to the north and the Tarim Basin to the south (Fig. 1b). In the central part of the

81　Tian Shan, several intramontane basins are preserved such as the Yili, Bayanbulak and Turfan basins

82　(Fig. 1 and 2). The Tian Shan Range is limited by large crustal thrusts verging northward in the north

83　and southward in the south towards the Junggar and Tarim Basins respectively (Fig. 1b). During the

84　Palaeozoic, several accretion events gave rise to an important topography that was progressively

85　eroded from Middle Triassic to Middle Jurassic (e.g. Dumitru et al., 2001; Li et al., 2004; Jolivet et al.,

86　2010; 2013; Yang et al., 2013; S. Liu et al., 2013). The present-day topography formed later, mostly

87　through the Cenozoic reactivation of Late Palaeozoic tectonic structures, driven by the far-field

88　effects of the India-Asia collision event (e.g. Tapponnier and Molnar, 1979; Windley et al., 1990; Allen

89　et al., 1991; Hendrix et al., 1994; Glorie et al., 2010; De Grave et al., 2011, 2013). Whereas the

90　present-day topography is believed to have developed since Late Oligocene – Miocene (e.g. Charreau

91　et al., 2005, 2009, 2012), uncertainties remain about the topographic evolution of the range during

92　the Jurassic - Early Palaeogene period. For example, while low-thermochronology data suggest a long

93 tectonic quiescence during most of the Mesozoic leading to very slow and constant exhumation
94 within the range (Dumitru et al., 2001; Jolivet et al., 2010; 2013), Upper Jurassic alluvial fan deposits
95 exposed in the foothills are interpreted as the consequence of a compressive reactivation of the
96 range (Hendrix et al., 1992; Li et al., 2004). In this context, the present study on calcretes and nodules
97 provides independent information on the palaeo-topographic evolution of the area.

98

3. Field work and samples

3.1 Field description

101   Throughout the area, we recognized several calcareous features (calcretes and nodules) at
102 distinct stratigraphic levels (Fig. 2). Very few age data are available due to the lack of clear marine
103 deposits, the scarcity of interbedded volcanic levels and the very limited available palynological and
104 faunistic data (e.g. Wang and Gao, 2012; Yang et al., 2013). Nevertheless regional stratigraphic
105 correlations can be made using available geological maps and the stratigraphic columns presented in
106 published palynoflora and vertebrate studies (e.g. Eberth et al., 2001; Bian et al., 2010; Jiang et al.,
107 2008; Heilbronn, 2014), as well as our own observations.

108   Below is a short description of the stratigraphy and the inferred associated depositional
109 environments (Heilbronn, 2014). The present-day semi-arid climate of this region offers excellent
110 outcrops preservation and exposure. In the northern foothills, from west to east (Fig. 1), the Wusu
111 section exposes 1650 m of Middle Jurassic to Upper Cretaceous series, the Manas section exposes
112 8100 m of Triassic to Neogene series and the Qiu Er Gou section exposes 55 m of late Upper
113 Cretaceous deposits. In the Bayanbulak intramontane basin (Fig. 1), 620 m of Jurassic to Neogene
114 series are exposed, the stratigraphic continuity of which remains questionable. Finally, in the
115 southern foothills, the Yaha section provides 2800 m of Jurassic to Neogene deposits.

116   The Mesozoic series of the Tian Shan area are constituted of continental deposits (Hendrix et
117 al., 1992; Li et al., 2004; Jiang et al., 2008; Li and Peng, 2010). These series are mainly composed of
118 stream and alluvial plain deposits (few decimetres- to a few metre-thick grey and red sandstone
119 beds) alternating with floodplain or lake deposits (clays and siltstones). Thick conglomerates which
120 deposited in an alluvial fan environment are exposed at the end of the Upper Jurassic and the Upper
121 Cretaceous series (Fig. 2).

4

122 Calcareous features are mainly recognized at two intervals: the late Middle Jurassic to Lower
123 Cretaceous and the late Upper Cretaceous to Palaeocene. The most continuous level of neo-formed
124 carbonate is located in the later. This calcrete consists of a several metres thick indurated and white
125 layer, parallel to the bedding and laterally continuous over tens of kilometres (Fig. 3a). The calcrete is
126 commonly associated with conglomeratic beds (host rock), consisting in matrix-supported
127 conglomerates with sub-angular to sub-rounded pebbles (Fig. 3b). Carbonate nodules are white,
128 crumbly to highly indurated, spherical to elongated concretions of micritic carbonate (few
129 centimetres in diameter), and either occur as disseminated bodies in red silty to sandy levels or form
130 coalescent beds. Such a feature is classical for pedogenic carbonate (see Fig. 3E in Li et al., 2013). On
131 several locations, one can observe a vertical transition from a zone enriched in nodules towards the
132 massive calcrete layer (Fig. 3c); both features thus likely represent two stages of calcification,
133 complete for calcrete, incipient for nodules. Processes controlling the formation of massive calcretes
134 are still discussed and it is likely that both phreatic and pedogenic processes are involved (e.g.
135 Wright, 2008 and references therein).

136 Moreover some limestone beds occur in the silty to sandy alternations of the late Middle Jurassic
137 continental series of the Yaha section (Fig. 2) (e.g. Jiang et al., 2008). They are white to dark grey in
138 colour, several centimetres- to several decimetres-thick and rather continuous laterally (Fig. 3d) and
139 often show evidence of bioturbation (burrows). Middle Jurassic brackish water incursions have been
140 inferred along the southern margin of the Junggar Basin (Chen and Zhang, 2000; Sha et al., 2011; Pan
141 et al., 2013). We thus analysed those limestone beds in order to check their possible marine origin,
142 even if they are interbedded with sediment series described as continental deposits (Hendrix et al.,
143 1992; Sobel,1999; Jiang et al., 2008).

144

3.2 Sampling strategy

146 The recognition of nodules and calcrete layers in several places throughout the Tian Shan
147 Range and their localization in the same stratigraphic levels (Upper Jurassic, Upper Cretaceous) offer
148 a unique opportunity to specify the palaeo-topographic evolution of the area during the late
149 Mesozoic. Every observed type of carbonated pedogenic feature has been sampled. Samples were
150 first collected along a north-south transect across the Tian Shan, mostly focusing on the Manas,
151 Bayanbulak and Yaha sections. For the Upper Cretaceous level, five to six samples have been
152 collected from each section (Table 1; Fig. 2). When the calcrete and nodules were present together
153 in a single site, both were sampled as they might have formed under distinct pedogenic conditions,

154   even if some continuity between the two types of objects has been locally observed (Fig. 3c). For the

155   Jurassic period, the sampling is not fully complete since calcification has not been observed in the

156   Bayanbulak section and is only poorly developed in the Manas and Wusu sections.

157   On the northern foothills, six samples were also collected from the Qiu Er Gou section only

158   20 km east of the Manas section (Fig. 1). Calcification in these two close-by sites is located in the

159   Upper Cretaceous series and likely developed under identical climatic and topographic conditions.

160   They thus allow specifying the isotopic heterogeneities solely associated with the calcification

161   processes. For example, evaporation can induce kinetic effects that modify the $\delta^{18}O$ signature of

162   pedogenic carbonates (Ufnar et al., 2008 and references therein).

163   Finally, several late Middle Jurassic limestone beds have been sampled on the Yaha section

164   (Fig. 3d) both in order to confirm or infirm their suspected lacustrine origin using the isotopic tool,

165   and to use their isotopic composition as a complementary proxy to palaeo-environmental

166   reconstruction (e.g. Li et al., 2013).

167

3.3 Sample description and preparation

169   A total of 32 fist-sized samples have been collected (Fig. 4). Calcrete samples consist of

170   conglomerates in which the matrix has been cemented by neo-formed calcite (Fig. 4a). Figure 4a

171   shows white calcite cement that precipitated around the pebbles. This cement has been sampled by

172   scraping or micro-drilling and reduced to powder for isotopic analysis. Since the conglomerates

173   contain some detrital fragments of carbonate rocks, special care was taken to avoid contamination of

174   the sampled powder by pebble-derived carbonate. In one sample of the Manas section (sample MC

175   11-3; Table 1), three types of neo-formed carbonates were observed and sampled: calcitic cement

176   (fraction A), a few millimeters wide veinlets (fraction B) and millimetric geodic calcite grains (fraction

177   C).

178   Nodule samples consist of nearly pure neo-formed calcite, sometimes easily extracted from their

179   sandy to silty host rock (Fig. 4b). These nodules were crushed and neo-formed calcite was separated

180   by hand-picking from remaining small detrital grains. For both the calcrete and nodule samples, the

181   separated calcite was then crushed in a boron carbide mortar before analysis.

182 Limestone samples sometimes contain some detrital materials, but no pebble was observed.

183 Centimetre-sized fragments of limestones have been detached from the samples, crushed in an

184 Abiche mortar, then in a boron carbide mortar to get a finely grained powder.

185

4. Analytical techniques

187 The stable isotope analysis was performed at the stable isotope laboratory of Geosciences

188 Rennes, University of Rennes 1. About 12 mg of calcite powder have been reacted with anhydrous

189 H_3PO_4 for a few hours at 50°C. The liberated CO_2 was analysed on a VG Optima triple collector mass

190 spectrometre. Routine analysis of in-house standard (Prolabo Rennes) and international standards

191 NBS 18 and NBS 19 ensures accuracy of the results. The global precision is estimated at ± 0.15‰ for

192 oxygen (SMOW) and ± 0.10‰ for carbon (PDB). Isotopic results are reported using the conventional

193 "delta" notation in Table 1 and summarized in Figure 5, where they are compared with data from the

194 literature.

195

5. Results

197 In Table 1, for the Qiu Er Gou section where calcrete and nodules have been collected in

198 nearby horizons, there is no significant isotopic difference between the two facies. These two

199 components are thus not distinguished in Figure 5a.

200 The analytical data are rather clustered (our data shown in black and grey on Fig. 5), with

201 some points lying outside of the main field. The data for calcrete and nodules are shown in Figure 5a

202 and those for limestones in Fig. 5b. On the Manas section, the lowest $\delta^{18}O$ value (19.2‰) was

203 measured for the geodic calcite (sample MC 11-3A, see Fig. 5a), suggesting that this calcite

204 developed under physicochemical conditions distinctly different from the ones prevailing during the

205 main calcification event. On the same section, the Palaeogene nodule MC 11-SED-6 (see Fig. 5a) is

206 somewhat different from the others, displaying lower $\delta^{18}O$ (20.4‰) and $\delta^{13}C$ (-6.1‰) values. On the

207 Yaha section, the two Jurassic nodules (YA 12-SED-39 and 41, see Fig. 5a) display extreme $\delta^{13}C$ values,

208 respectively of -7.6 and -2.0‰. Similarly, the Lower Cretaceous nodule (YA 12-CHIM-1, see Fig. 5a) is

209 also distinguishable from the Upper Cretaceous – Lower Palaeogene calcrete by higher $\delta^{18}O$ (24.6‰)

210 and $\delta^{13}C$ (-2.98‰) values. On the Yaha section, while the calcrete displays homogeneous isotopic

7

211 compositions, the nodules show wider isotopic ranges and only the Palaeogene nodule YA 12-SED-
212 19A (see Fig. 5a) shows a composition identical to that of the Yaha calcrete.

213 However, in spite of these differences, the Upper Cretaceous - Lower Palaeogene calcrete
214 and nodules of the Tian Shan display rather homogeneous oxygen and carbon isotope compositions,
215 irrespective of the sampling site. Fluctuations are small in comparison to the range of possible values.

216 Indeed, most of the Upper Cretaceous - Lower Palaeogene calcrete and nodule $\delta^{18}O$ values
217 are between 21 and 25‰ (SMOW), while most of the $\delta^{13}C$ values are between -4 and -6‰ (PDB) (Fig.
218 5a). On the other hand, the Tian Shan calcrete and nodules differ overall from other calcretes in
219 China (Early Cretaceous in age; Li et al., 2013) by lower $\delta^{13}C$ values and more homogeneous
220 compositions.

221 Finally, the Middle Jurassic limestone beds from the Yaha section have highly variable oxygen
222 and carbon isotope composition: $\delta^{18}O$ values are between 18 and 23‰ (SMOW) and $\delta^{13}C$ values are
223 between -3.5 and +3.1‰ (PDB), well outside the field of unaltered marine limestones (Fig. 5b). When
224 compared to the lacustrine limestones analysed by Li et al. (2013), the values obtained in the Yaha
225 limestones fall within the field of the SE China and NW China data. We thus interpret those
226 limestones as lacustrine deposits.

227

6. Discussion

229 The stable isotope dataset presented here allow us discussing several characteristics of the
230 palaeo-environmental evolution of the Chinese Tian Shan. Indeed, the isotope compositions of the
231 pedogenic carbonates formed in equilibrium with soil or ground water are believed to record a
232 significant part of the original signature of the water, which is itself influenced by several
233 geographical and morphological parameters: continentality, latitude and altitude. Consequently,
234 besides climatic evolution, any topographic changes across space or through time will induce an
235 evolution in the isotopic record.

236 The Yaha section provides a record of calcification conditions in both the Late Jurassic and
237 the Late Cretaceous - Early Palaeogene times, which helps discussing the evolution of the southern
238 foothills during the Late Mesozoic. The pre-requisite of such analyses is that calcification developed
239 soon after sediment deposition. Although there is no indication for this in the Tian Shan, the nodules
240 were often found in close association with the calcrete (Fig. 3c) and were thus very likely developed

8

close to the surface. Only the small geodic calcite with an oxygen isotope composition distinct from the whole nodule and calcrete population (sample MC 11-3A) obviously developed in association with some diagenetic event, after the main calcification phase. This shows that the diagenetic circulations that occurred in the series induced isotopic deviation strong enough to be recorded in our data. To a first order, excluding these data (see sample MC 11-3A), it is thus reasonable to discuss the Late Cretaceous - Early Palaeogene palaeo-climatic and palaeo-topographic characteristics, using calcretes and nodules that developed at this stratigraphic level. Finally, some aspects linked to the process of calcification itself can be discussed.

6.1 Isotopic variability within a calcification site

As previously mentioned, numerous processes can influence the isotopic values of pedogenic carbonates (e.g. Ufnar et al., 2008; Charreau et al., 2012; Li et al., 2013), independently of the initial composition of the meteoric water. Some effects are related to the hydrological conditions (evaporation, respiration, seasonality) and influence the oxygen isotopic record. Others are linked to the nature of the palaeo-flora and the relative amount of organic carbon over inorganic carbon hosted in limestones which are mostly of marine origin. It is far beyond the scope of this study to discuss the impact of each of these processes on the isotopic composition of the nodules and calcrete that we measured (the reader is invited to refer to the exhaustive discussion developed in Ufnar et al., 2008; Charreau et al., 2012; Li et al., 2013). Instead, we sampled two neighbouring sites (the Manas and Qiu Er Gou sections) in the northern foothills in order to specify the range of isotopic heterogeneity associated with the calcification processes in our study area. The range of values of the Qiu samples are 21.4 to 24.6‰ (δ^{18}O) and -4.29 to -6.14‰ (δ^{13}C), while the range of the Manas samples are 19.2 to 25.3‰ (δ^{18}O) and -3.75 to -6.08‰ (δ^{13}C). We consider these ranges as quite comparable.

Each site displays a similar range in δ^{18}O values for the Upper Cretaceous - Lower Palaeogene calcrete and nodules (δ^{18}O between 22 and 25.3‰ for the Manas site, between 21.4 and 24.6‰ for the Qiu Er Gou site; Table 1). The δ^{13}C values are also comparable (δ^{13}C between -3.7 and -4.9‰ for the Manas site, between -4.3 and -6.0‰ for the Qiu Er Gou site). The carbonation processes acting at both sites were thus nearly identical, inducing comparable isotopic heterogeneity.

Also, some neo-formed carbonates display specific isotopic compositions in relation to original textural characteristics. The most obvious one is the geodic calcite that developed in the calcrete of the Manas section (MC 11-3A). This calcite has a δ^{18}O of 19.2‰ which is lower than that one of its calcrete host (22.2‰). Two main factors can lower the δ^{18}O value of carbonate. Firstly, the

9

273 δ^{18}O value of the fluid may have been 3‰ lower when the geode developed than when the calcrete

274 formed. Secondly, the isotopic fractionation is inversely correlated with temperature. Assuming a

275 constant δ^{18}O value of the water from which precipitation occurred, a higher temperature of

276 precipitation during the formation of the geode could result in a lower δ^{18}O value of the calcite. We

277 favor this second hypothesis for two reasons. Firstly, lowering the δ^{18}O value of the original meteoric

278 water would imply a drastic change in palaeo-climate or palaeo-environmental conditions between

279 the calcrete stage and the geodic stage, a set of conditions that should be recorded by other proxies

280 like the sedimentological record itself and in neighbor areas of Central Asia, which is not the case

281 (e.g. Li et al., 2004). Secondly, a decrease of 3‰ of the δ^{18}O value of calcite corresponds to an

282 increase of the temperature of calcite precipitation of about 12-15°C: if calcrete precipitated at 20°C,

283 which corresponds reasonably to pedogenic carbonation conditions, the geode may have

284 precipitated at about 32-35°C. This temperature increase may correspond to burial of the series of a

285 few hundreds of metres within a normal geothermal gradient, a burial that actually occurred in the

286 area during the Cenozoic. Therefore, the geodic calcite developed under late diagenetic conditions

287 rather than under early pedogenic ones.

288

289

290 *6.2 Temporal evolution on the southern foothills (Yaha section)*

291 Along the Yaha section, the calcification features formed merely during the Late Jurassic and

292 the Late Cretaceous - Early Palaeogene. These pedogenic carbonates suggest that both periods were

293 characterized by a similar semi-arid climate (e.g. Hendrix et al., 1992; Li et al., 2004; Sun and Wang,

294 2005). Moreover, the oxygen isotope composition of the neo-formed carbonates is comparable: from

295 21.2 to 22.6‰ for the Jurassic, and from 21.6 to 23.4‰ for the Early Palaeogene, which is again

296 consistent with similar climatic conditions. In fact, the Late Cretaceous sample YA-12-CHIM-1 displays

297 a δ^{18}O value (24.6‰) slightly above the other Yaha samples.As we have only one sample for this

298 intermediate stratigraphic level, we can hardly consider this single value as representative of a

299 regional palaeo-environmental event. It remains that the homogeneity of the stable isotope

300 compositions of the calcification features studied here may indicate that our samples underwent

301 comparable in-situ processes such as evaporation. This homogeneity also suggests that the

302 composition of the rainwater, and by inference also the fundamental parameters evaporation,

303 continentality, latitude, and altitude were likely comparable in the Yaha region for the Late Jurassic

304 and Early Palaeogene periods. In other words, based on our isotopic data no major palaeo-

305 geographic changes occurred during this period in the Yaha region (confirms earlier data published
306 by Li et al., 2004), i.e. no significant topographic variations occurred either by relief building or
307 destruction. Furthermore, the transgression of the Paratethys Sea from the West into the Tarim
308 Basin during the Late Cretaceous (e.g. Sobel, 1999) had no influence on the conditions of
309 development of pedogenic carbonates in the Yaha section.

310

311   In the Yaha region, the isotopic compositions of the Middle Jurassic limestones are different
312 from those of marine limestones of the same age elsewhere in the world (Veizer et al., 1999) (Fig.
313 5b). It could be argued that these limestones were originally marine and that subsequent diagenesis
314 affected their primary compositions, as known for many carbonate platforms (e.g. Brigaud et al.,
315 2009). However, the fact that δ^{13}C of the limestones is highly variable and that the δ^{13}C values are
316 not correlated with the δ^{18}O values, does not plead for such a diagenetic modification of marine
317 limestones. Indeed, the δ^{18}O values of the limestones ranging between 18 and 23‰, the large δ^{13}C
318 variation with both positive and negative values and the lack of correlation between the oxygen and
319 carbon signatures are common features of lacustrine carbonates (e.g. Li et al., 2013 and references
320 therein). These authors provided a very detailed discussion on the use of these isotopic signatures in
321 terms of palaeo-environmental reconstructions. In the present work, it would be hazardous to
322 develop such a discussion because of the rather small number of isotopic data. Our inference that
323 the limestone beds are lacustrine is consistent with the silty to sandy continental nature of the series
324 in which they are inter-bedded (see field description above and in Hendrix et al., 1992; Sobel, 1999;
325 Jiang et al., 2008; Heilbronn, 2014).

326

6.3 Palaeo-topography during the Late Cretaceous - Early Palaeogene period

328   We have analysed calcification features in three Upper Cretaceous - Lower Palaeogene series
329 in the north, the south and within the Tian Shan Range. Currently, there are two first order
330 differences between the northern and southern sides of the range (Charreau et al., 2012): 1) the
331 cumulative meteoric precipitation rate is much higher on the northern side; i.e., between 100 and
332 250 mm/year in the southern Junggar Basin than on the southern side of the Tian Shan; i.e., less than
333 40 mm/year in the Tarim Basin, and 2) the mean δ^{18}O value of meteoric water is lower than -8‰ on
334 the northern side and higher than this value on the southern side. If a significant palaeo-topography

11

335 existed during the Late Cretaceous - Early Palaeogene period, such an isotopic gradient in meteoric

336 water compositions likely existed and should have been recorded in pedogenic carbonates.

337 From the lithological point of view, our field observation showed that calcrete features

338 developed mainly in conglomerates, i.e. on rocks with comparable porosity and permeability

339 properties. Also, a semi-arid climate prevailed over the whole study area in order to develop

340 pedogenic carbonates (e.g. Hendrix et al., 1992). It is then reasonable to think that the prominent

341 variable that could have been recorded by the carbonates developed in the Upper Cretaceous -

342 Lower Palaeogene series, is the initial isotopic composition of the meteoric water, a property that

343 depends primarily on the origin of atmospheric masses (e.g. Charreau et al., 2012). In Table 1 and

344 Figure 5, there is no significant isotopic difference between the Upper Cretaceous - Lower

345 Palaeogene pedogenic carbonates of the northern, central and southern parts of the present-day

346 Tian Shan Range. The interpretation that immediately comes out is that the meteoric waters were

347 identical in the three regions.

348 The easier way to reach identical values is to consider that these meteoric waters originated

349 from the same oceanic reservoir and underwent the same atmospheric evolution. The Paratethys sea

350 in the West-Tarim Basin (e.g. Dercourt et al., 1993; Mao and Norris, 1988) could be a possible source

351 of these meteoritic waters. Regardless of the marine source of meteoric waters, there is no isotopic

352 evidence for the existence of any orographic barrier between the studied sections at the time of

353 calcification. If the latter rapidly followed deposition, there was no significant relief in that area at

354 the Cretaceous - Palaeogene boundary.

355

356

7. Conclusion

358 Pedogenic carbonates (calcrete and nodules) and limestone beds have been identified and

359 analysed for $\delta^{18}O$ and $\delta^{13}C$ on two main stratigraphic levels of the Tian Shan Mesozoic-Cenozoic

360 series (Late Jurassic and Late Cretaceous - Early Palaeogene). The limestone beds are restricted to

361 the Middle Jurassic series of the southern foothills and are probably of lacustrine origin. The oxygen

362 and carbon isotope compositions of the pedogenic carbonates are homogeneous in both the

363 southern and northern foothills of the Tian Shan Range, as well as in the intramontane Bayanbulak

364 Basin. Palaeo-environmental conditions of pedogenic carbonates development were thus identical

365 on a regional scale during the Late Cretaceous - Early Palaeogene period. No significant palaeo-relief

366 existed by that time in the area, implying that the actual Tian Shan topography mostly results from

367 the Cenozoic reactivation event.

368

369

370

376

References

378 Allen, M.B., Windley, B.F., Zhang Chi, Zhao Zhong-yan, Wang Guang-Rei, 1991. Basin evolution within

379 and adjacent to the Tien Shan Range, NW China. J. Geol. Soc. Lond. 148, 369–378.

380 Alonso-Zarza, A.M., 2003. Palaeoenvironmental significance of palustrine carbonates and calcretes in

381 the geological record. Earth-Sci. Rev. 60, 261–298.

382 Ashraf, A.R., Sun, Y., Sun, G., Uhl, D., Mosbrugger, V., Li, J., Herrmann, M., 2010. Triassic and Jurassic

383 palaeoclimate development in the Junggar Basin, Xinjiang, Northwest China—a review and additional

384 lithological data. Palaeobiodiversity Palaeoenvironments 90, 187–201.

385 Bian, W., Hornung, J., Liu, Z., Wang, P., Hinderer, M., 2010. Sedimentary and palaeoenvironmental

386 evolution of the Junggar Basin, Xinjiang, Northwest China. Palaeobiodiversity Palaeoenvironments

387 90, 175–186.

388 Brigaud, B., Durlet, C., Deconinck, J.-F., Vincent, B., Thierry, J., Trouiller, A., 2009. The origin and

389 timing of multiphase cementation in carbonates: Impact of regional scale geodynamic events on the

390 Middle Jurassic Limestones diagenesis (Paris Basin, France). Sediment. Geol. 222, 161–180.

391 Charreau, J., Chen, Y., Gilder, S., Barrier, L., Dominguez, S., Augier, R., Sen, S., Avouac, J.-P., Gallaud,

392 A., Graveleau, F., Wang, Q., 2009. Neogene uplift of the Tian Shan Mountains observed in the

393 magnetic record of the Jingou River section (northwest China). Tectonics 28, TC2008.

394 Charreau, J., Chen, Y., Gilder, S., Dominguez, S., Avouac, J., Sen, S., Sun, D., Li, Y., Wang, W., 2005.

395 Magnetostratigraphy and rock magnetism of the Neogene Kuitun He section (northwest China):

396 implications for Late Cenozoic uplift of the Tianshan mountains. Earth Planet. Sci. Lett. 230, 177–192.

13

397 Charreau, J., Kent-Corson, M.L., Barrier, L., Augier, R., Ritts, B.D., Chen, Y., France-Lannord, C.,
398 Guilmette, C., 2012. A high-resolution stable isotopic record from the Junggar Basin (NW China):
399 Implications for the paleotopographic evolution of the Tianshan Mountains. Earth Planet. Sci. Lett.
400 341, 158–169.

401 Chen, J.-H., Zhang, Y.-J., 2000. Marine bivalves found in Lower Jurassic of continental Junggar Basin of
402 west China. Xinjiang Geol. 18, 28–31.

403 De Grave J., Glorie, S., Buslov, M.M., Izmer, A., Fournier-Carrie, A., Batalev, V.Y., Vanhaecke, F.,
404 Elburg, M., Van den haute, P., 2011. The thermo-tectonic history of the Song-Kul plateau, Kyrgyz Tien
405 Shan: Constraints by apatite and titanite thermochronometry and zircon U/Pb dating. Gondwana
406 Research 20, 745-763.

407 De Grave J., Glorie, S., Buslov, M.M., Stockli, D.F., McWilliams, M.O., Batalev, V.Y., Van den haute, P.,
408 2013. Thermo-tectonic history of the Issyk-Kul basement (Kyrgyz Northern Tien Shan, Central Asia).
409 Gondwana Research 23, 998-1020.

410 Dercourt, J., Ricou, L.-E., Vrielynck, B., 1993. Atlas Tethys, Paleoenvironmental Maps: Explanatory
411 Notes. Gauthier-Villars.

412 Dumitru, T.A., Zhou, D., Chang, E.Z., Graham, S.A., Hendrix, M.S., Sobel, E.R., Carroll, A.R., 2001.
413 Uplift, exhumation, and deformation in the Chinese Tian Shan. Geol. Soc. Am. Mem. 194, 71 –99.

414 Eberth, D.A., Brinkman, D.B., Chen, P.-J., Yuan, F.-T., Wu, S.-Z., Li, G., Cheng, X.-S., 2001. Sequence
415 stratigraphy, paleoclimate patterns, and vertebrate fossil preservation in Jurassic–Cretaceous strata
416 of the Junggar Basin, Xinjiang Autonomous Region, People's Republic of China. Can. J. Earth Sci. 38,
417 1627–1644.

418 Garzione, C.N., Dettman, D.L., Quade, J., DeCelles, P.G., Butler, R.F., 2000. High times on the Tibetan
419 Plateau: Paleoelevation of the Thakkhola graben, Nepal. Geology 28, 339–342.

420 Glorie, S., De Grave, J., Buslov, M.M., Elburg, M.A., Stockli, D.F., Gerdes, A., 2010. Multi-method
421 chronometric constraints on the evolution of the Northern Kyrgyz Tien Shan granitoids (Central Asian
422 Orogenic Belt): From emplacement to exhumation. Journal of Asian Earth Sciences 38, 131-146.

423 Hasiotis, S.T., Kraus, M.J., Demko, T.M., 2007. Climatic controls on continental trace fossils. Trace
424 Foss. Concepts Probl. Prospects Elsevier Amst. 172–195.

425 Heilbronn, G., 2014. Palaeogeographic and palaeotopographic evolution of the Chinese Tian Shan
426 during the Mesozoic. Thèse - Université de Rennes 1, 267 p.

427 Hendrix, M.S., 2000. Evolution of Mesozoic Sandstone Compositions, Southern Junggar, Northern
428 Tarim, and Western Turpan Basins, Northwest China: A Detrital Record of the Ancestral Tian Shan. J.
429 Sediment. Res. 70, 520–532.

430 Hendrix, M.S., Dumitru, T.A., Graham, S.A., 1994. Late Oligocene-early Miocene unroofing in the
431 Chinese Tian Shan: An early effect of the India-Asia collision. Geology 22, 487-490.

1
2
3
4
5
6
7
8
9
10
11
12
13
14
15
16
17
18
19
20
21
22
23
24
25
26
27
28
29
30
31
32
33
34
35
36
37
38
39
40
41
42
43
44
45
46
47
48
49
50
51
52
53
54
55
56
57
58
59
60
61
62
63
64
65

432 Hendrix, M.S., Graham, S.A., Carroll, A.R., Sobel, E.R., McKnight, C.L., Schulein, B.J., Wang, Z., 1992.
433 Sedimentary record and climatic implications of recurrent deformation in the Tian Shan: Evidence
434 from Mesozoic strata of the north Tarim, south Junggar, and Turpan basins, northwest China. Geol.
435 Soc. Am. Bull. 104, 53 –79.

436 Jiang, D.-X., Wang, Y.-D., Robbins, E.I., Wei, J., Tian, N., 2008. Mesozoic non-marine petroleum source
437 rocks determined by palynomorphs in the Tarim Basin, Xinjiang, northwestern China. Geol. Mag. 145,
438 868–885.

439 Jolivet, M., Dominguez, S., Charreau, J., Chen, Y., Li, Y., Wang, Q., 2010. Mesozoic and Cenozoic
440 tectonic history of the central Chinese Tian Shan: Reactivated tectonic structures and active
441 deformation. Tectonics 29, TC6019.

442 Jolivet, M., Heilbronn, G., Robin, C., Barrier, L., Bourquin, S., Guo, Zh., Jia, Y., Guerit, L., Yang, W., Fu
443 B., 2013. Reconstructing the Late Palaeozoic – Mesozoic topographic evolution of the Chinese Tian
444 Shan: available data and remaining uncertainties. Advances in Geosciences 37, 7-18.
445

446 Jolivet, M., Barrier, L., Dominguez, S., Guerit, L., Heilbronn, G., Fu, B., 2014. Unbalanced sediment
447 budgets in the catchment – alluvial fan system of the Kuitun River (northern Tian Shan, China):
448 Implications for mass-balance estimates and erosion rates in mountain ranges. Geomorphology 214,
449 168-182.
450 Li, X., Xu, W., Liu, W., Zhou, Y., Wang, Y., Sun, Y., Liu, L., 2013. Climatic and environmental indications
451 of carbon and oxygen isotopes from the Lower Cretaceous calcrete and lacustrine carbonates in
452 Southeast and Northwest China. Palaeogeogr. Palaeoclimatol. Palaeoecol. 385, 171–189.

453 Li, Z., Peng, S., 2010. Detrital zircon geochronology and its provenance implications: responses to
454 Jurassic through Neogene basin-range interactions along northern margin of the Tarim Basin,
455 Northwest China. Basin Res. 22, 126–138.

456 Li, Z., Song, W., Peng, S., Wang, D., Zhang, Z., 2004. Mesozoic–Cenozoic tectonic relationships
457 between the Kuqa subbasin and Tian Shan, northwest China: constraints from depositional records.
458 Sediment. Geol. 172, 223–249.

459 Liu, D., Jolivet, M., Yang, W., Zhang, Z., Cheng, F., Zhu, B., Guo, Z., 2013. Latest Paleozoic–Early
460 Mesozoic basin–range interactions in South Tian Shan (northwest China) and their tectonic
461 significance: Constraints from detrital zircon U–Pb ages. Tectonophysics 599, 197–213.

462 Liu, S., Su, S., Zhang, G., 2013. Early Mesozoic basin development in North China: Indications of
463 cratonic deformation. J. Asian Earth Sci. 62, 221–236.

464 Mao, S., Norris, G., 1988. Late Cretaceous-early Tertiary dinoflagellates and acritarchs from the Kashi
465 area, Tarim Basin, Xinjiang Province, China. Life Science Contributions, 150 Royal Ontario Museum, ,
466 93p.

467 Pan, Y., Sha, J., Wang, Y., Zhang, X., Yao, X., Peng, B., Rao, X., 2013. The brackish-water bivalve
468 Waagenoperna from the Lower Jurassic Badaowan Formation of the Junggar Basin and its
469 palaeoenvironmental and palaeogeographic significance. Geosci. Front. 4, 95–103.

15

470 Pustovoytov, K.E., 2002. Pedogenic carbonate cutans on clasts in soils as a record of history of
471 grassland ecosystems. Palaeogeogr. Palaeoclimatol. Palaeoecol. 177, 199–214.

472 Retallack, G.J., 1997. Colour guide to paleosols. John Wiley, Chichester [England]; New York, 175 p.

473 Sha, J., Vajda, V., Pan, Y., Larsson, L., Yao, X., Zhang, X., Wang, Y., Cheng, X., Jiang, B., Deng, S., Chen,
474 S., Peng, B., 2011. Stratigraphy of the Triassic–Jurassic Boundary Successions of the Southern Margin
475 of the Junggar Basin, Northwestern China. Acta Geol. Sin. - Engl. Ed. 85, 421–436.

476 Sobel, E.R., 1999. Basin analysis of the Jurassic–Lower Cretaceous southwest Tarim basin, northwest
477 China. Geol. Soc. Am. Bull. 111, 709–724.

478 Sun, X., Wang, P., 2005. How old is the Asian monsoon system?—Palaeobotanical records from
479 China. Palaeogeogr. Palaeoclimatol. Palaeoecol. 222, 181–222.

480 Tapponnier, P., Molnar, P., 1979. Active faulting and Cenozoic tectonics of the Tien Shan, Mongolia,
481 and Baykal regions. J. Geophys. Res. 84, 3425–3459.

482 Ufnar, D.F., Gröcke, D.R., Beddows, P.A., 2008. Assessing pedogenic calcite stable-isotope values: Can
483 positive linear covariant trends be used to quantify palaeo-evaporation rates? Chem. Geol. 256, 46–
484 51.

485 Veizer, J., Ala, D., Azmy, K., Bruckschen, P., Buhl, D., Bruhn, F., Carden, G.A.F., Diener, A., Ebneth, S.,
486 Godderis, Y., Jasper, T., Korte, C., Pawellek, F., Podlaha, O.G., Strauss, H., 1999. 87Sr/86Sr, δ13C and
487 δ18O evolution of Phanerozoic seawater. Chem. Geol. 161, 59–88.

488 Vincent, S.J., Allen, M.B., 2001. Sedimentary record of Mesozoic intracontinental deformation in the
489 eastern Junggar Basin, northwest China: Response to orogeny at the Asian margin. Geol. Soc. Am.
490 Mem. 194, 341 –360.

491 Wang, S.-E., Gao, L.-Z., 2012. SHRIMP U-Pb dating of zircons from tuff of Jurassic Qigu Formation in
492 Junggar Basin, Xinjiang. Geol. Bull. China 31, 503–509.

493 Windley, B.F., Allen, M.B., Zhang, C., Zhao, Z.-Y., Wang, G.-R., 1990. Paleozoic accretion and Cenozoic
494 redeformation of the Chinese Tien Shan Range, central Asia. Geology 18, 128–131.

495 Wright, V.P., 2008. Calcrete, in: Nash, D.J., McLaren, S.J. (Eds.), Geochemical Sediments and
496 Landscapes. Blackwell Publishing Ltd, pp. 10–45.

497 Wright, V.P., Tucker, M.E., 1991. Calcretes. Blackwell Scientific Publications, Oxford, 1-22.

498 Yang, W., Jolivet, M., Dupont-Nivet, G., Guo, Z., 2014. Mesozoic-Cenozoic tectonic evolution of
499 southwestern Tian Shan: evidence from detrital zircon U/Pb and apatite fission track ages of the
500 Ulugqat area, Northwest China. Gondwana Res. 26, 986-1008.

501 Yang, W., Jolivet, M., Dupont-Nivet, G., Guo, Z., Zhang, Z., Wu, C., 2013. Source to sink relations
502 between the Tian Shan and Junggar Basin (northwest China) from Late Palaeozoic to Quaternary:
503 evidence from detrital U-Pb zircon geochronology. Basin Res. 25, 219–240.

16

504

Table caption

506 Table 1- Oxygen and carbon isotope composition of the pedogenic and lacustrine carbonates from

507 the Tian Shan Range.

508

509 **Figure caption**

510 Fig. 1- a) Schematic tectonic map of Asia and location of the Tian Shan Range in Central Asia. b) Map

511 of the Tian Shan area (DEM, G-TOPO-30, Mercator projection) showing the five sampling sites: the

512 Wusu, Manas and Qiu Er Gou sections on the northern foothills, the Bayanbulak section in the

513 Bayanbulak intramontane basin, and the Yaha section on the southern foothills of the range. Section

514 location and GPS coordinates are given in Table 1.

515

516 Fig. 2- Synthetic figure showing (top) the present-day topographic profile through the Tian Shan

517 Range, together with the five sampling sites (black dots; W. = Wusu; M. = Manas; Q. = Qiu Er Gou; B.

518 = Bayanbulak; Y. = Yaha). (left) General lithological column (C = Clay, s = Silt, Sf = Fine sand, Sm =

519 Medium sand, Sc = Coarse sand, g = Gravel, P = Pebble, B= Boulder) derived from our field

520 observations of the Middle Jurassic to Palaeocene series from the Yaha section (southern foothills).

521 This column shows the general trends and types of Mesozoic deposits around the Tian Shan Range

522 and is consistent with the work of Hendrix et al. (1992). The correspondence between lithological

523 limits and stratigraphic ages relies on the available geological maps, previous studies (Hendrix et al.,

524 1992) and our field work (J1 = Early Jurassic; J2 = Middle Jurassic; J3 = Late Jurassic; K1 = Early

525 Cretaceous; K2 = Late Cretaceous; P = Palaeocene). (right) Type and stratigraphic position of the neo-

526 formed carbonates.

527

528 Fig. 3- Outcrop views. a) Landscape view of the sampled 8 metre-thick massive calcrete, which runs

529 over tens of kilometres laterally (Late Cretaceous – Early Palaeocene, top of the Manas Section). b)

530 Detailed view of the massive conglomeratic calcrete (hammer for scale). The boundaries of the

531 carbonate body correspond to lithological limits between sandy layers and gravel-rich layers. c)

532 Transition from nodule-rich layers into a massive calcrete (Late Cretaceous – Early Palaeocene, Yaha

17

533 Section; hammer for scale). d) Decimetric grey to white limestone layers. These layers are not easily

534 distinguishable solely from their colour.

535

536 Fig. 4- Examples of studied samples. a) Conglomeratic massive calcrete (sample MC 11 4; Late

537 Cretaceous – Early Palaeocene; Manas section). b) Centrimetre-sized calcareous nodules (sample B

538 11 SED 1; Early Palaeocene; Bayanbulak section). c) Limestone, locally with shales or terrigenous

539 input (sample YA 12 SED 1; Middle Jurassic; Yaha section).

540

541 Fig. 5- δ^{13}C (PDB) vs. δ^{18}O (SMOW) diagram of the pedogenic carbonates (a) and the limestones (b) of

542 the Tian Shan Range. The isotopic compositions of Lower Cretaceous pedogenic carbonates and

543 limestones from China are shown for comparison (data from Li et al., 2013). The field of Jurassic

544 marine limestones of the world is indicated in grey (Veizer et al., 1999).

Table

Sample	Type	Formation	Coordinates		Calcite	
			Latitude	Longitude	$\delta^{18}O$	$\delta^{13}C$
WUSU						
WE 12 SED 1	Calcar. nodules	Jurassic (J3)	44° 8'20,90"N	84°30'19,70"E	21.2	-4.96
MANAS						
MC 11 SED 6	Calcar. nodules	Palaeogene	43°57'55,08"N	85°48'28,08"E	20.4	-6.08
MC 11 5	Calcrete	Cret./Palaeogene	idem		25.3	-3.75
MC 11 4	Calcrete	Cret./Palaeogene	idem		23.7	-4.22
MC 11 3C	Calcrete (matrix)	Cret./Palaeogene	idem		22.2	-4.05
MC 11 3B	Calcrete (vein)	Cret./Palaeogene	idem		22.1	-4.87
MC 11 3A	Calcrete (geode)	Cret./Palaeogene	idem		19.2	-4.73
MC 11 2	Calcrete	Cret./Palaeogene	43°57'42,72"N	85°48'27,60"E	22.0	-4.67
QIU ER GOU						
HU 12-SED 12	Calcar. nodules	Cret./Palaeogene	43°52'3,00"N	86°23'32,30"E	21.4	-5.19
HU 12-SED 11	Calcar. nodules	Cret./Palaeogene			23.3	-6.02
HU 12-SED 10	Calcrete	Cret./Palaeogene			24.6	-4.29
HU 12-SED 9	Calcrete	Cret./Palaeogene			23.0	-4.99
HU 12-SED 8	Calcar. nodules	Cret./Palaeogene			22.8	-5.33
HU 12-SED 7	Calcrete	Cret./Palaeogene	43°52'2,40"N	86°23'29,50"E	22.7	-6.14
BAYANBULAK						
B 11 SED 1	Calcar. nodules	Palaeogene?	43° 4'23,52"N	84°17'6,66"E	22.3	-4.65
B 11 SED 06	Calcrete	Cret./Palaeogene?	idem		23.1	-5.31
B 11 SED 02	Calcrete	Cret./Palaeogene?	idem		23.0	-5.79
B 11 SED 05	Calcrete	Cret./Palaeogene?	idem		24.3	-5.32
B 11 SED 04	Calcrete	Cret./Palaeogene?	43° 4'21,96"N	84°17'5,52"E	23.0	-5.53
YAHA						
YA 12 SED 19 A	Calcar. nodules	Palaeogene	42° 4'52,32"N	83°15'48,20"E	23.4	-4.10
YA 12 SED 18	Calcrete	Cret./Palaeogene	42° 4'56,30"N	83°15'48,20"E	22.7	-4.75
YA 12 SED 17	Calcrete	Cret./Palaeogene	42° 4'57,15"N	83°15'48,61"E	22.7	-4.95
YA 12 SED 13	Calcrete	Cret./Palaeogene	42° 4'56,84"N	83°15'50,13"E	21.6	-4.13
YA 12 SED 16	Calcrete	Cret./Palaeogene	42° 4'57,32"N	83°15'50,13"E	21.7	-3.86
YA 12 CHIM 1	Calcar. nodules	Cretaceous (K1)	42° 5'47,80"N	83°16'40,10"E	24.6	-2.98
YA 12 SED 41	Calcar. nodules	Jurassic (J3)	42° 6'52,30"N	83°17'18,50"E	21.2	-2.03
YA 12 SED 39	Calcar. nodules	Jurassic (J2-J3)	42° 6'57,90"N	83°17'18,10"E	22.6	-7.61
YA 12 SED 38	Limestone	Jurassic (J2)	idem		20.1	-3.16
YA 12 SED 37	Limestone	Jurassic (J2)	idem		19.2	-0.26
YA 12 SED 36	Limestone	Jurassic (J2)	idem		18.5	0.20
YA 12 SED 34	Limestone	Jurassic (J2)	idem		23.0	3.14
YA 12 SED 33	Limestone	Jurassic (J2)	42° 7'3,37"N	83°17'7,09"E	17.7	-0.37
YA 12 SED 1	Limestone	Jurassic (J2)	42° 7'32,40"N	83°14'10,40"E	20.4	-3.49

Figure 1
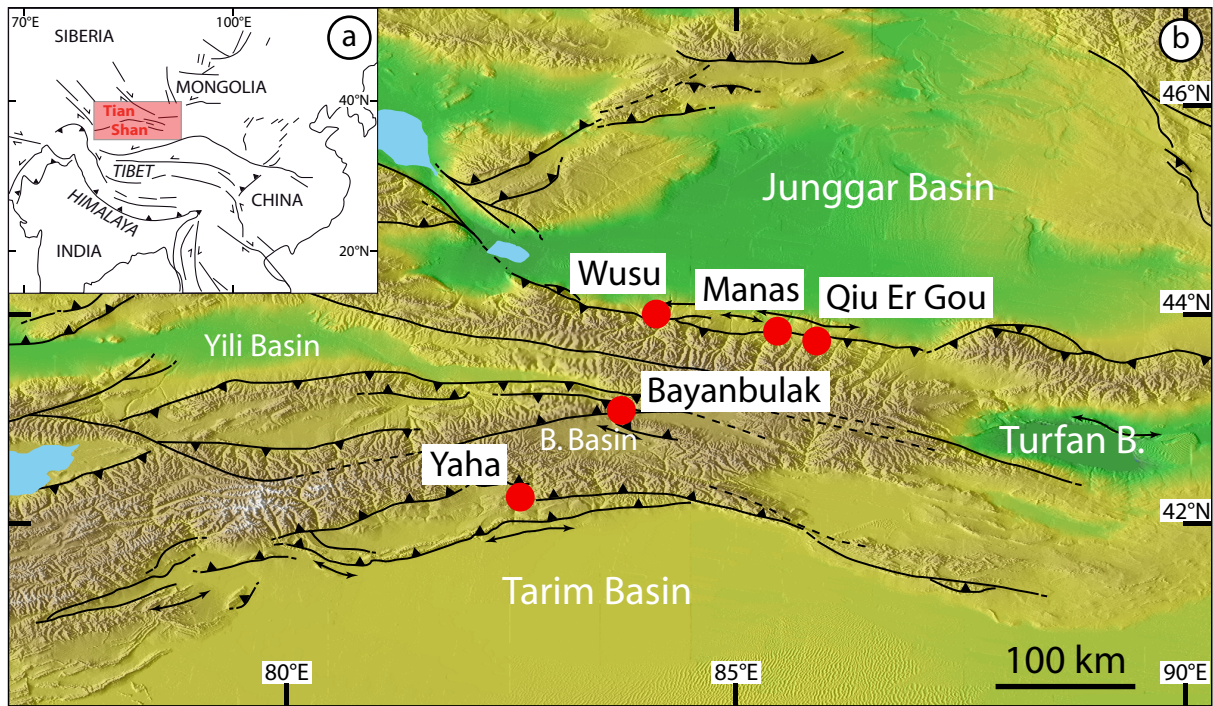
Heilbronn et al., 2014 - Fig. 1
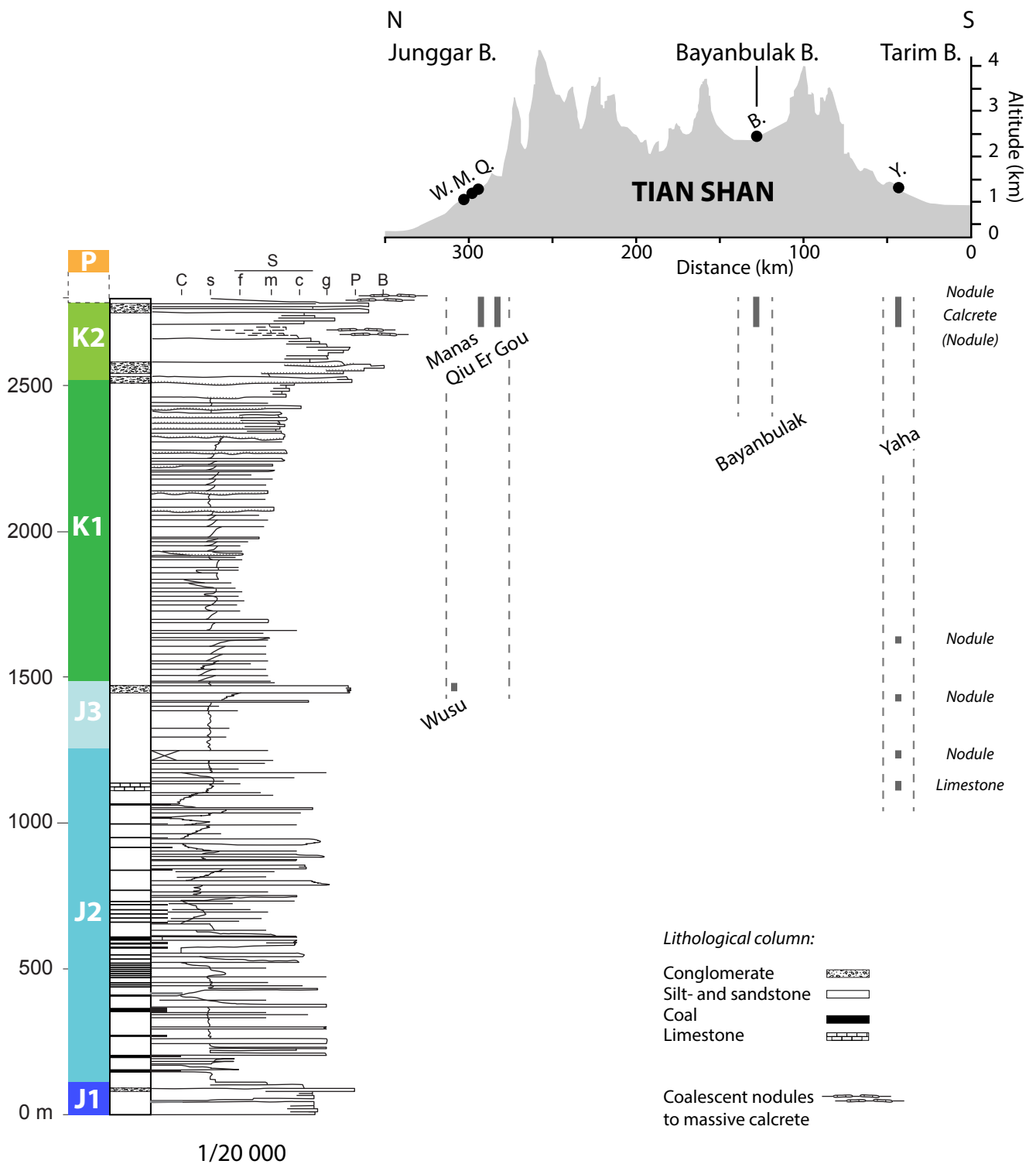
Figure 2

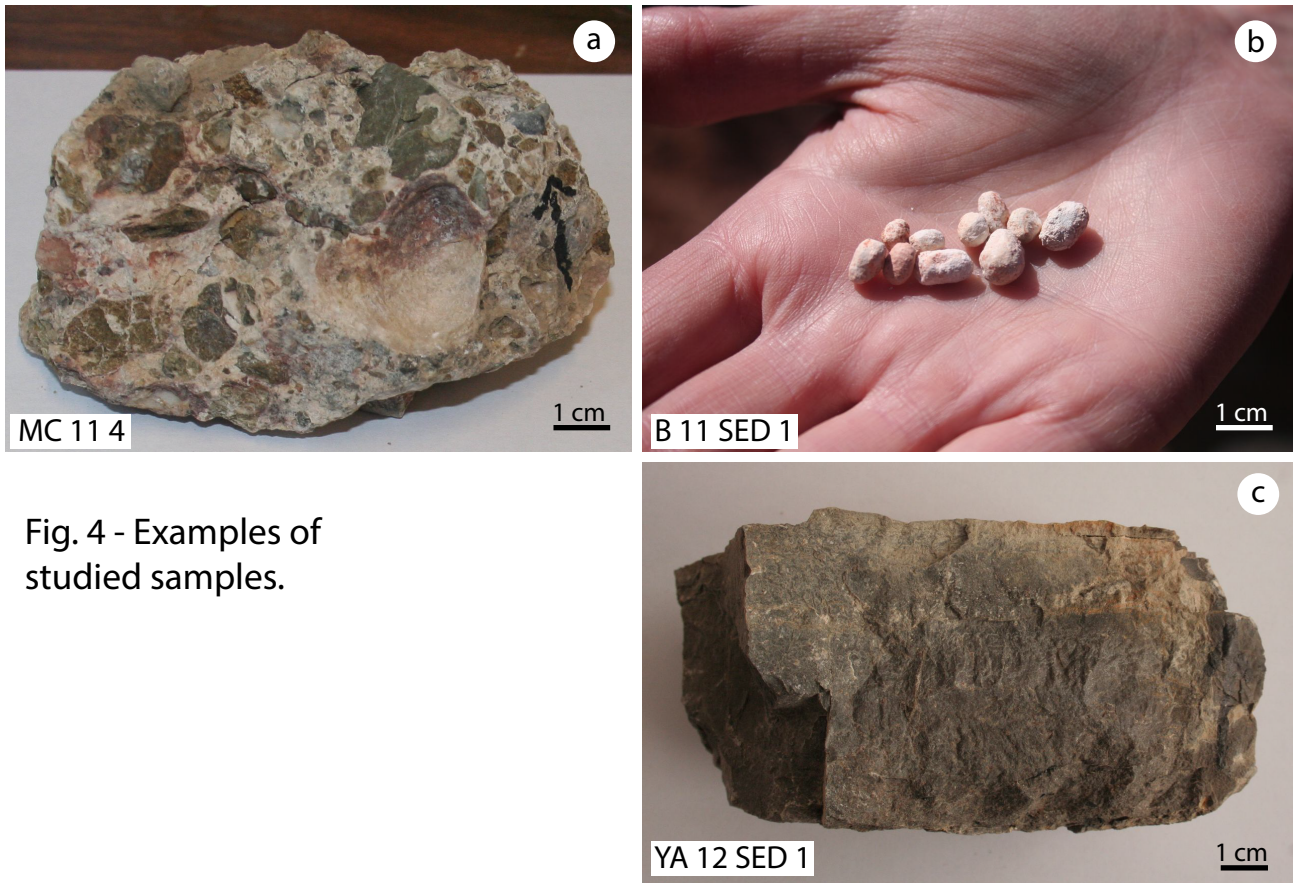# Heilbronn et al., 2014 - Fig. 2
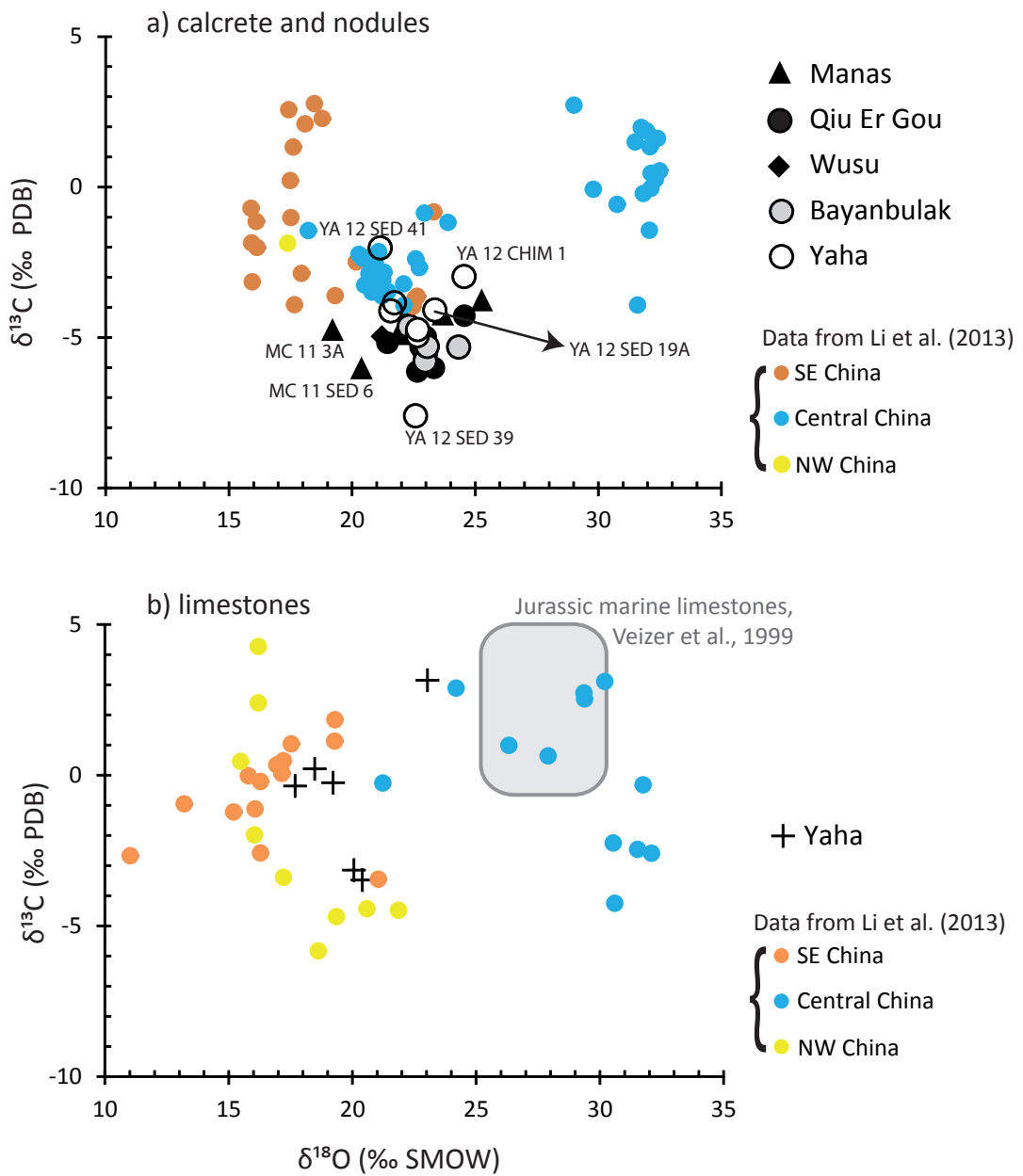
Figure 3

Fig. 3 - Outcrop-views.

Heilbronn et al., 2014 - Fig. 3

Figure 4

Fig. 4 - Examples of studied samples.

Heilbronn et al., 2014 - Fig. 4

Figure 5

a) calcrete and nodules

b) limestones

Heilbronn et al., Figure 5